J. Am. Soc. Mass Spectrom. (2017) 28:498–506
DOI: 10.1007/s13361-016-1582-y

RESEARCH ARTICLE

Spontaneous Mass and Charge Losses from Single Multi-Megadalton Ions Studied by Charge Detection Mass Spectrometry

David Z. Keifer, Andrew W. Alexander, Martin F. Jarrold

Chemistry Department, Indiana University, 800 E Kirkwood Ave., Bloomington, IN 47405, USA

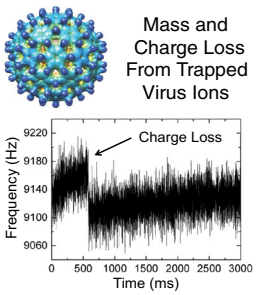

Abstract. Spontaneous mass and charge losses from individual multi-megadalton ions have been observed with charge detection mass spectrometry (CDMS) by trapping single hepatitis B virus (HBV) capsids for 3 s. Gradual increases in the oscillation frequency of single ions in the ion trap are attributed mainly to mass loss (probably solvent, water, and/or salt). The total mass lost during the 3 s trapping period peaks at around 20 kDa for 4 MDa HBV $T = 4$ capsids. Discrete frequency drops punctuate the gradual increases in the oscillation frequencies. The drops are attributed to a sudden loss of charge. In most cases a single positive charge is lost along with some mass (on average around 1000 Da). Charge loss occurs for over 40% of the trapped ions. It usually occurs near the beginning of the trapping event, and it occurs preferentially in regions of the trap with strong electric fields, indicating that external electric fields promote charge loss. This process may contribute to the decrease in *m/z* resolution that often occurs with megadalton ions.

Keywords: Charge detection mass spectrometry, Dissociation, Megadalton ions, Charge loss

Received: 22 October 2016/Revised: 14 December 2016/Accepted: 16 December 2016/Published Online: 12 January 2017

Introduction

Electrospray mass spectrometry (ES-MS) is the premier method for determining accurate masses of protein complexes and other supramolecular assemblies. An analyte ionized by ES picks up a distribution of charges, and examining the location of each peak in the *m/z* spectrum provides the mass. This is not possible for many highly-charged megadalton-sized complexes because the peaks are unresolved [1, 2]. Most mass spectrometers should be able to resolve the charge state peaks, but the peaks are broadened [3–5]. Understanding the nature of the peak broadening is thus of great importance for the analysis of high-mass ions. Solvent adducts make an important contribution to the peak broadening. For native mass spectrometry, the solvent is water and a volatile salt, usually ammonium acetate.

Several features enhance desolvation. Raising the pressure and mass of the gas in the first differentially pumped regions of a mass spectrometer collisionally cools the kinetic energy picked up in the supersonic expansion into the instrument and improves desolvation [6–9]. Desolvation is also assisted by heating the inlet [10]. Using nano-ES instead of regular ES has several benefits as well [11, 12], the most important being that the primary droplets from nano-ES are about an order of magnitude smaller than from regular ES.

As solvent evaporates from an ES droplet its radius decreases, and the charge density increases. Eventually, the surface tension of the droplet is overcome by electrostatic repulsion and a fission event occurs, reducing the charge. The number of charges that can be accommodated on the droplet before a fission event is the Rayleigh limit,

$$z_R = \frac{8\pi}{e}\left(\gamma\varepsilon_0 R^3\right)^{1/2} \quad (1)$$

where R is the droplet radius, γ is the surface tension, ε_0 is vacuum permittivity, and e is the charge on an electron [13]. The ES charging mechanism depends on the analyte. Large, near-spherical objects are thought to be charged by the charge residue mechanism (CRM) [14], where the particle remains in the interior of the electrospray droplet while the droplet evaporates and undergoes multiple fission events until, finally, the remaining charge is deposited on the mostly desolvated analyte ion. The maximum charge that a spherical particle of radius R can acquire by the CRM is the Rayleigh limit.

Correspondence to: Martin F. Jarrold; *e-mail:* mfj@iu.edu

For small droplets, the electric field at the surface can become strong enough to eject single ions [15, 16]; the ion-emission mechanism (IEM) then takes over and controls the charge [17]. The transition to the IEM is predicted to occur near a radius of 5 nm for ammonium acetate droplets [18, 19]. For larger objects, the charge is controlled by the Rayleigh limit, whereas for smaller objects it is determined by the IEM. The hepatitis B virus (HBV) capsids studied here have radii of ~14.5 and ~16 nm for $T = 3$ and $T = 4$ capsids, respectively [20], so the IEM should not play a role.

A change in the mass or charge of a trapped ion can be monitored using charge detection mass spectrometry (CDMS). In CDMS both the m/z and charge of individual ions are measured simultaneously. The ion passes through a metal tube and the induced charge is detected by a charge-sensitive preamplifier [21, 22]. The magnitude of the induced charge provides the charge of the ion, and the time-of-flight through the tube provides its m/z. The uncertainty in the charge measurement is high for single pass experiments (usually hundreds of elementary charges [23–26]) which limits the mass resolution. The charge can be measured much more precisely by embedding the detector tube inside an ion trap so that the ion's induced charge is measured repetitively [27–31]. The m/z in ion-trap CDMS is determined by the ion's oscillation frequency. Only one ion is trapped and measured at a time, so ion-trap CDMS is quite slow, but it is capable of providing near perfect charge accuracy [31].

Since a single ion can be trapped for at least several seconds, each ion's m/z and charge can be tracked as a function of time. The m/z decreases gradually, which we attribute to evaporation of residual solvent (water and/or salt). In addition, over 40% of the ions exhibit sudden losses of a single charge. Smith and coworkers have performed related work by trapping single ions in an FTICR cell and shifting their charge states with a reagent [32–34]. In these experiments, only the m/z was measured and the charge was deduced from the shifts in the m/z values for different charge states. Only a few ions were trapped and measured because these experiments are time consuming. More recently, Anderson and coworkers have trapped single quantum dots in a 3D quadrupole ion trap and measured the rate of their mass loss from laser heating [35–37]. In the 1990s, the Smith group also observed spontaneous shifts in the m/z of individual DNA ions trapped for several minutes, but whether the shifts were due to changes in charge or mass could not be determined [38]. To our knowledge, spontaneous changes in mass or charge of trapped macromolecular ions have not been studied since.

Experimental

Charge Detection Mass Spectrometer

Our charge detection mass spectrometer has been described thoroughly elsewhere [2, 28–31]. Ions are generated with positive-mode nano-ES and are drawn through a heated capillary into the first differentially pumped region, which contains an ion funnel. Ions are transmitted into subsequent differentially pumped regions containing first a hexapole (with a 100 V DC offset to set the ion's kinetic energy) and then an rf-only quadrupole. From there, an Einzel lens focuses the ions into the entrance of a dual hemispherical deflection analyzer (HDA), which passes ions within a narrow range of kinetic energies per charge, centered at 100 eV/z. Ions exiting the HDA enter the final differentially pumped region, which contains an ion trap with conical endcaps and a central, shielded detector tube that is connected to a cryogenically cooled JFET (2SK152) at the input of a charge-sensitive preamplifier (Amptek A250, Bedford, MA, USA).

To trap an ion, the potential on the back endcap is first raised from ground to 135 V and then, 0.5 ms later, the potential on the front endcap is raised to 135 V. After a predetermined time, both endcaps are grounded for 0.5 ms to clear the trap, and then the next trapping event begins. In this study, ions were trapped for up to 2991 ms. When the endcaps are grounded, the ions pass through the trap and impinge on a pair of microchannel plates (MCPs). The MCP output is used to control the ion beam intensity and maximize the chance of trapping a single ion. Events with no ions or with multiple ions are discarded by the analysis program. Trapped ions oscillate back and forth through the detector tube and induce a signal on each pass.

The time domain signal is analyzed by a FORTRAN program. The program starts by performing a fast Fourier transform (FFT) on the entire trapping event to determine the number of ions trapped. This single FFT cannot be used to measure the charge on the ion because the magnitude of the peaks in the FFT are proportional to the time the ion is trapped; the full-event FFT does not account for ions that are not trapped the full time. If a single ion is detected, a short, Gaussian-apodized FFT is stepped across the trapping event. The center of the fundamental peak in the FFT determines the frequency of the ion, f, which is related to the m/z of the ion by

$$f = \sqrt{\frac{C}{E^{1.8}} \frac{z}{m}} \tag{2}$$

where C is a calibration constant determined from Simion simulations, and E is the ion energy per charge (nominally 100 eV/z).

The magnitudes of the fundamental and the second harmonic peaks are added to determine the charge [31]. The signature of an ion being lost from the trap is the loss of the fundamental peak from the short FFTs. Normally, the m/z and charge measurements are averaged over the time that the ion is trapped, and then the average m/z and charge are multiplied to obtain the mass. The process is repeated for thousands of ions, and the results are binned into a mass histogram. Here the methodology has been modified slightly since we are focusing on changes in frequency and charge over time; the particulars are described below.

Sample Preparation

A 40 μM solution of truncated, assembly-competent core protein dimer of hepatitis B virus (HBV) in 50 mM HEPES pH 7.5 was assembled into empty capsids in 300 mM NaCl for 24 h. HBV is dimorphic. The core proteins used here assemble into a mixture of $T = 3$ and $T = 4$ capsids [39] weighing around 3 and 4 MDa, respectively. The solution was dialyzed into 100 mM ammonium acetate. Size-exclusion chromatography was then performed to transfer the capsids into high-purity ammonium acetate (>99.9%, Sigma-Aldrich, St. Louis, MO, USA).

Results and Discussion

Figure 1 shows representative frequency versus time plots for two trapped HBV $T = 4$ capsid ions, obtained by stepping a short FFT across the time domain signal. In Figure 1a, the oscillation frequency gradually increases and approaches an asymptotic value at long times. According to Equation 2, a frequency increase can be explained by the loss of mass or kinetic energy or by a gain of charge. The net positive charge of a trapped ion can increase by release of a negative ion. However, this is very unfavorable from an electrostatic point of view, and we show below that changing the charge by just 1 e (elementary charge) has a very obvious signature. The kinetic energy of a trapped ion can decrease through collisions with the background gas, by interactions with the charge induced on the detector tube, or by the loss of mass. Solvent (water and/or salt) molecules can be lost if the ion is not completely desolvated.

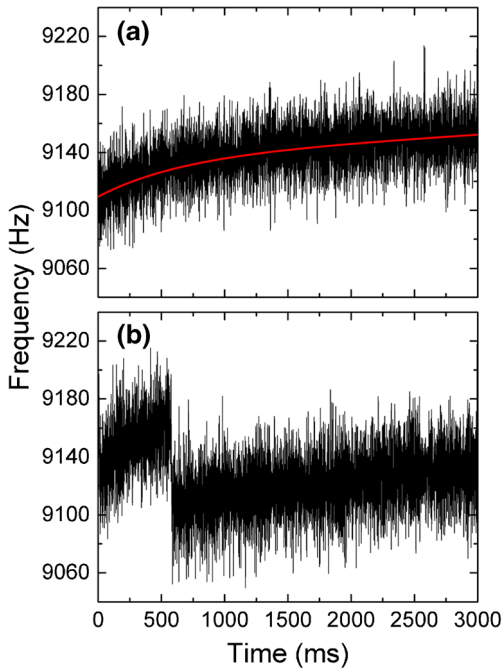

Figure 1. Representative frequency versus time plots for single HBV $T = 4$ capsid ions. **(a)** Typical result for an ion with constant charge. The gradual increase in frequency is from solvent (water and/or salt) evaporation and from energy loss due to collisions with the background gas. **(b)** Typical result for an ion which loses a single charge just after 500 ms of being trapped, indicated by the sudden drop in frequency

Collisions with a background gas results in an exponentially decaying energy [7, 40]. This can be adapted to describe the kinetic energy per charge as a function of time,

$$E = E_i e^{-2t/\tau} \tag{3}$$

where E is kinetic energy per charge after time t, E_i is initial kinetic energy per charge, and τ is given by

$$\tau = \frac{3\,m}{4\,m_g\,n\,\sigma\,v_{kT}} \tag{4}$$

where m_g is the mass of the background gas molecules, n is the number density of the gas, σ is the collision cross section of the particle with the gas, and v_{kT} is the thermal velocity of the background gas. Substituting Equation 3 into Equation 2 gives the ion's frequency in the trap as a function of time accounting for background gas collisions. The resulting equation has a positive second derivative, while the results in Figure 1a show that the ion's oscillation frequency has a negative second derivative. Thus, energy loss through collisions with the background gas alone cannot account for the experimental observations.

Incorporating mass loss can produce functions with the correct shape. Models describing evaporation rates of droplets in vacuum, for which the rate of mass loss is proportional to the radius of the droplet [41] do not apply to our case since even a monolayer of water on the HBV capsid surface would weigh many hundreds of kilodaltons. It will become clear below that this is much greater than the observed mass loss. Moreover, the frequency as a function of time arising from this type of mass loss has a second derivative very near 0 for realistic parameters. Thus, this is not an appropriate model for multiple reasons.

We now consider a model where solvent molecules independently desorb from equivalent sites on the capsid surface. We assume that the heat reservoir provided by the capsid is sufficiently large that loss of a comparatively small number of solvent molecules does not affect the temperature. With this model, the mass at time, t, is given by

$$m = \left(m_i - m_p\right) e^{-k(T)t} + m_p \tag{5}$$

where m_i is the initial mass of the particle including excess solvent, m_p is the final mass, and $k(T)$ is the first order rate constant for evaporation of the excess solvent. At $t = 0$, $m = m_i$, and as t approaches infinity, $m = m_p$. In addition to reducing the mass, the mass loss will decrease the capsid's kinetic energy per charge. The decrease in energy depends on the electric potential at the ion's location in the trap when the evaporation event occurs. For example, assuming the ion initially has a kinetic energy of 100 eV/z at a potential of 0 V, if it loses a solvent molecule where the potential is 100 V (i.e., where the ion is reflecting in the trap and is momentarily stationary), the ion will still be accelerated through a 100 V field in the trap and will still have a kinetic energy of 100 eV/z at 0 V. On the other

hand, if the ion loses mass in the detector tube (where the potential is nominally 0 V), its energy loss is proportional to its mass loss. The kinetic energy per charge of the ion at 0 V as a result of mass loss is thus given by,

$$E = (E_i - V)\frac{m}{m_i} + V \tag{6}$$

where E_i is the ion's initial kinetic energy per charge at 0 V and V is electric potential where the evaporation event occurs. Equation 5 can be substituted into Equation 6 to give an expression for the kinetic energy per charge as a function of time as a result of mass loss. However, it is important to consider whether Equation 6 should be modified to account for energy loss from collisions and from the interaction between the ion's charge and the induced charge. Although not the primary factors explaining our changes in frequency, they may still make a significant contribution.

For HBV capsid ions with nitrogen background gas at 2.7×10^{-9} Torr, the pressure in the trap for these experiments, the time constant for energy decay from collisions, τ in Equation 3, is ~3000 s. An ion with an initial energy of 100 eV/z would therefore lose about 0.2 eV/z throughout a 3 s trapping event. While this seems like a modest loss of energy, it turns out to be quite important.

Calculating the effect of the charge-induced charge interaction is more complicated. To understand the effect of the induced charge on the ion's kinetic energy, first imagine a simplified case where the charge-sensitive preamplifier is detached from the detector tube, and the detector tube is initially at 0 V. As a positive ion approaches, it polarizes the tube, inducing a negative charge on the inside surface, and a positive charge on the outside. The negative surface charge on the inside of the tube accelerates the ion and increases its kinetic energy. If the ion is on the tube axis so that the charge is evenly distributed and does not exert a net force, the kinetic energy of the ion will remain constant while it is in the tube. Upon exiting the tube, the kinetic energy of the ion decreases as it moves away from the induced surface charge and the surface charges on the inside and outside of the of the tube rebalance. In this case, the interaction between the charge and the induced charge has no net effect on either the energy of the ion or the overall charge on the tube.

In reality, the detector tube has both capacitance and resistance to ground through the preamplifier, making an RC circuit. As with the simplified case above, the ion polarizes the tube as it approaches, inducing a negative charge inside and a positive charge outside. While the ion is in the tube, the charge on the outside of the tube (which is equal in magnitude and polarity to the charge on the ion) flows into the relatively low impedance of the preamplifier input where it is mostly stored on the feedback capacitor. This charge is then returned to the tube as the ion exits. However, a small portion of the positive charge is lost to the feedback resistance during the transit time, resulting in a net negative charge on the tube when the charges re-balance as the ion exits. The deceleration of the ion as it exits the tube is now greater than the acceleration it received when it entered, which results in a net loss of kinetic energy for the ion. While trapped, an ion spends about 30% of its time in the detector tube [31] so after the ion exits, there is time for the tube to return to its original potential before the ion returns.

The change in the voltage of the tube due to the induced charge can be calculated from the amplifier gain, and then the change in the voltage of the tube during the ion's passage can be calculated from the time constant of the RC circuit, the frequency of the ion's oscillation, and the duty cycle. For the ions studied here, the voltage on the tube drops by about 1 nV while the ion passes through it, leading to a net decrease of the ion's kinetic energy per charge of 1 neV/z with each pass. Even for the tens of thousands of passes, the ions undergo during a 3 s trapping event, the total energy loss is still only tens of microvolts. Thus, the effect of the ion's collisions with the background gas is about 10^4 times more important than the effect of the charge-induced charge interaction. As a result, Equation 6 should be modified to include the effects of collisions, but the effects of the charge-induced charge interaction can be ignored.

Equation 7 results from combining Equations 3, 5, and 6 and describes the ion's energy as a function of time as a result of mass loss from solvent evaporation and collisions with background gas.

$$E = \left[\frac{E_i - V}{m_i}\left[(m_i - m_p)e^{-k(T)t} + m_p\right] + V\right] e^{-t/\tau} \tag{7}$$

Note that m, which varies with time here, is also in Equation 4 for τ. However, including this time dependence explicitly has a negligible impact on the results; therefore, we simply use the initial mass of the particle (m_i) in Equation 4.

Substituting Equations 5 and 7 into Equation 2 yields the following expression,

$$f = \sqrt{\frac{Cz}{(m_i - m_p)e^{-k(T)t} + m_p}}\left(\left[\frac{E_i - V}{m_i}\left[(m_i - m_p)e^{-k(T)t} + m_p\right] + V\right]e^{-t/\tau}\right)^{-0.9} \tag{8}$$

which provides the oscillation frequency of a trapped ion as a function of time, accounting for first-order loss of solvent and loss of energy due to background gas collisions. The electric potential is a function of time because the ion is oscillating through the trap, but using the time-weighted average electric potential that a trapped ion experiences (46.9 V for the trap used here) is a good approximation. The energies calculated with reasonable parameters using Equation 7 and assuming a constant, average electric potential, differ from calculations where the variations in the electric potential are treated explicitly by only around 1–100 ppm.

Equation 8 has a negative second derivative with respect to time for reasonable input parameters, so it is a candidate to model gradual frequency shifts such as in Figure 1a. The red

curve in this figure is in fact the best fit using this model where the measured charge and mass were taken as initial guesses for z and m_i. C, E_i, and V were fixed, whereas z, m_i, m_p, and k were varied within reasonable limits. The best fit was achieved with m_i = 4.094 MDa and m_p = 4.082 MDa. A bare T = 4 HBV capsid should contain 120 capsid protein dimers and have a sequence mass of 4.025 MDa. The final mass, m_p, is significantly larger than the sequence mass. In other studies, we have observed that freshly assembled T = 4 capsids often contain more than the expected number of dimers and then relax back to the expected mass over time. The fit indicates that ~13 kDa of solvent evaporates away from the T = 4 ion while it is trapped. If the energy loss from collisions is not included in the fit, the model predicts the loss of ~20 kDa of solvent. It is therefore important to include the ~0.2 eV/z loss of energy from collisions. It is also clear from this result that continuous mass loss is essential to explain the observed increase in frequency. This conclusion is supported by other studies where the frequency increase was found to depend on the interface conditions. For example, heating the inlet [10] and increasing the pressure in the first two regions [6–9] of the instrument are both expected to improve desolvation. Much larger frequency increases are observed when those steps are not taken, indicating that there is more solvent evaporation when ions are not as thoroughly desolvated.

The sudden drop in frequency just after 500 ms in Figure 1b is another common phenomenon for HBV capsid ions. Note that both before and after the drop, a gradual increase in frequency is observed, similar to Figure 1a. At least one drop occurs for about 43% of the trapped HBV ions. More than one drop occurs for about 11%. A histogram of the trapping time where the drop occurs is given in Figure 2a. Clearly, these discrete drops are most likely to occur near the beginning of the trapping event. According to Equation 2, a discrete drop in frequency can only result from a sudden drop in charge or a sudden, substantial increase in mass or energy. There is no conceivable means for an ion in high vacuum to suddenly gain substantial energy or mass, leaving loss of charge as the only plausible explanation. To verify this, the average charge measured after the drop in frequency was compared with the average charge measured before the drop. This comparison was made for every ion where there was a frequency drop, and the results were binned into a histogram. The result is shown in the black trace of Figure 2b. This peak is symmetric and is centered at −1.0 e with a full width at half maximum (FWHM) of 2.1 e.

To ensure that this result was not an artifact of our analysis, the frequency plots for ions that did not undergo a drop were split and the charges before and after the split were compared. To be able to compare the width and the shape of the charge difference histograms, the files were split with approximately the same time distribution as the sudden frequency drops (Figure 2a). The red trace in Figure 2b is a histogram of the difference in charges for these trapping events. It is centered at +0.1 e and has a 2.0 e FWHM. The FWHM is almost the same as observed for trapping events where a sharp drop in

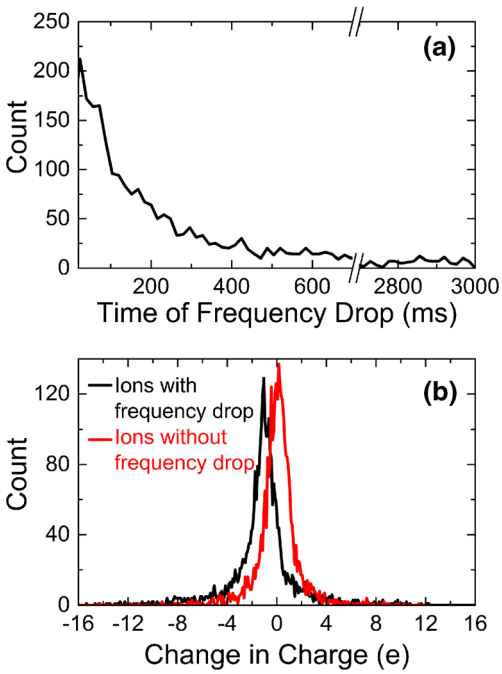

Figure 2. **(a)** Histogram of the times at which charge loss occurs. **(b)** The black trace is a histogram of the change in charge (final charge – initial charge) that occurs at the frequency drops. The red trace is the charge difference histogram for ions without a frequency drop, where the frequency versus time plots were randomly divided into initial and final regions according to the time distribution in part a)

frequency occurred (2.1 e). This indicates that the width of the charge histogram for the frequency drops is predominantly from the uncertainty in the measurement rather than from a distribution of charges being lost. The charge uncertainty improves with the square root of measurement time [30], and as evident from Figure 2a, the initial charge measurement is usually made over a short time. This leads to a relatively imprecise charge measurement, which results in the broad peaks in Figure 2b. The apparent slight increase in the average charge (0.1 e) noted above for ions that do not lose a charge is at least partially due to an artifact resulting from a change in the duty cycle of the signal [31]. As discussed above, solvent evaporation and background gas collisions throughout the 3 s trapping event decrease the energy over time. As the kinetic energy decreases, the ions do not penetrate as far into the endcaps of the trap, and the duty cycle changes slightly. On the other hand, the center of the peak from ions that do lose a charge is not offset from −1.0 e. This is probably because the loss of a charge increases the kinetic energy per charge, which offsets the energy loss from evaporation and collisions.

To summarize our conclusions to this point, the gradual increase in the frequency observed for all ions is attributed to solvent evaporation in conjunction with energy loss from collisions, and the sudden drops in frequency are assigned to the loss of a single positive charge. The next step is to determine how much mass is lost along with each charge. We start by determining the charges from the largest portions of the

trapping events that are uninterrupted by charge loss. The charges for other regions of the trapping events are then adjusted by 1 e increments based on this measurement. The initial m/z is determined from the first 100 frequency measurements (which corresponds to the first ~10 ms of trapping) assuming an energy of 100 eV/z. The initial mass is obtained from the initial charge multiplied by the initial m/z. The mass just before a charge loss event (m_f) is determined by iteratively solving

$$f_f = \sqrt{\frac{C}{\left(\left[(E_i - V)\frac{z_i}{z_f}\frac{m_f}{m_i} + V\right] e^{-t/\tau}\right)^{1.8}}\frac{z_f}{m_f}} \quad (9)$$

by adjusting m_f until the right side of the equation matches the measured frequency just before the charge loss event. Note that the energy loss due to collisions is accounted for by the exponential term in the denominator. In Equation 9, parameters with a subscript i are for the beginning of the trapping event, and parameters with subscript f correspond to the time just before the frequency drop. Equation 9 is similar to Equation 8, except that m_f in Equation 9 is not given by Equation 5. We use Equation 9 to model energy loss from collisions and solvent evaporation and then use the measured frequency and charge measurements to determine m_f. In other words, Equation 8 provides the theoretical basis that explains the raw frequency data, while Equation 9 is how the frequency and charge measurements are used to obtain an accurate mass at different times during a trapping event. Since the mass loss before the step in the frequency is due to continuous solvent evaporation, we can use the time-weighted average electric potential that the ion experiences in the trap for V in Equation 9 (46.9 V). Also, the charge is constant during these gradual frequency changes, so the charge just before the charge loss event, $z_f = z_i$, the initial charge.

In principle, Equation 9 could also be used to calculate how much mass is lost along with the single charge. In this case, the subscript i would now refer to the value of the parameter just before the charge loss and the f subscript would indicate the value just after the loss. However, a time-weighted average electric potential cannot be used in this case because the event is discrete and occurs at a particular electric potential, and we do not know where charge loss occurs for a particular ion.

To determine the mass lost with the charge, we start by defining the frequency shift as the difference between the oscillation frequencies before and after charge loss. Our approach is to compare the histogram of the frequency shifts for all ions that lose a charge (the solid black line of Figure 3a) with histograms of simulated frequency shifts for assumed mass losses. The histogram of the measured frequency shifts shows two peaks at around −35 and −87.5 Hz, with a low intensity region between them. To generate the histogram of simulated frequency shifts, we take the initial frequency and charge for each ion before the charge loss. When charge loss occurs, we calculate a final frequency assuming the loss of one charge along with a particular associated mass using Equation 9. As noted above, this requires information on the electric potential

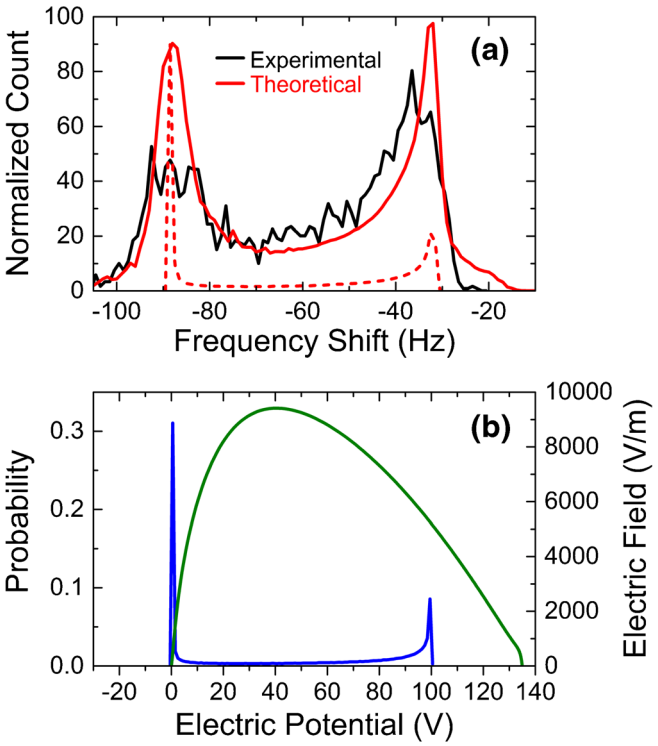

Figure 3. **(a)** Histograms of measured measured frequency shifts (solid black line). The dashed red line shows the simulated frequency shift histogram for an ion with an initial mass of 4.02 MDa, an initial charge of 146 e, and a mass loss of 1000 Da with the charge (see text). The solid red line shows the composite simulated frequency shift histogram determined by summing the simulated histograms calculated assuming a mass loss of 1000 Da with the charge, for all ions that show a frequency drop (see text). The composite and measured histograms are normalized to the same total areas. **(b)** The solid blue line shows the probability distribution of the electric potential experienced by a 100 eV/z ion oscillating in the trap. Substantial amounts of time are spent in or near the detector tube (close to 0 V) and near the reflection point (close to 100 V). The green line shows the electric field (right hand axis) experienced by the ions as a function of the electric potential

where the charge loss occurs. The blue line in Figure 3b shows the probability distribution of electric potentials experienced by a trapped ion. It was obtained by calculating the trajectory of a trapped ion with Simion 8.1 and tracking the electric potential at the ion's location at evenly spaced time steps. The ion spends nearly a third of its time near 0 V, which represents time spent in or near the detector tube, and it spends a substantial time near 100 V, where it reflects. Little time is spent at any particular potential between 0 V and 100 V. For each ion, the frequency shift is then calculated for thousands of potentials following the probability distribution shown in Figure 3b. This procedure neglects the fact that ions will reflect at lower electric potential as they lose energy from mass evaporation and collisions, but few ions have energies that drop below 99 eV/z, so this is not a serious concern. An example of a calculated frequency shift histogram for an ion with an initial mass and charge of 4.02 MDa and 146 e, which loses a mass of 1000 Da with the

charge, is shown as the dashed red line in Figure 3a. The frequency shift histogram corresponds closely to the electric potential probability distribution (blue line in Figure 3b). Simulated frequency shift histograms were calculated for all ions that show frequency drops using initial masses and charges from just before the drop, and then the individual histograms were summed to form a composite histogram. An example of a composite simulated frequency shift histogram is shown as the solid red line in Figure 3a. The composite histogram is normalized to the same area as the experimental one. The composite histogram is similar to the measured histogram; both show two peaks with intensity between them. For mass losses of between 0 and 2000 Da with the charge, both peaks move to less negative frequency shifts as the mass loss increases. However, the peak at around −87.5 Hz shifts by substantially more than the peak at −35 Hz, and so it is the location of the peak at around −87.5 Hz that provides the best information about the mass loss associated with the loss of a charge. From these simulations we estimate that the mass loss is 1000 ± 400 Da. The composite histogram shown in Figure 3a was calculated for a mass loss of 1000 Da. For mass losses less than 600 Da the composite histogram is too far to the left in Figure 3a, and for mass losses greater than 1400 Da it shifts too far to the right. The mass loss depends on the model used to describe the energy loss from collisions (Equation 3). Thus, the mass loss deduced here should be considered an estimate.

In addition to allowing an estimate of how much mass is lost with the charge, the simulations provide an explanation of the shape of the measured frequency shift histogram. The peak at around −87.5 Hz is from charge loss occurring at electric potentials near 0 V while the ion is in or near the detector tube, whereas the peak around −35 Hz is from charge loss at electric potentials near 100 V, which is in the endcap region of the trap, where the ions are turning-around.

The intensity in the measured histogram at around −87.5 Hz is significantly less than in the simulation. As noted above, the peak at −87.5 Hz is due to ions in and near the detector tube. The electric field in the detector tube is close to zero, so this raises the possibility that charge loss outside the detector tube is promoted by electric fields. The solid green line in Figure 3b shows the electric field (right hand axis) experienced by the ions as a function of the electric potential. In the regions of low electric field (corresponding to the peaks in the frequency shift histograms) the intensity in the measured histogram is less than in the simulated composite histogram. On the other hand, in regions of high electric field (between the peaks) the intensity in the measured histogram exceeds the intensity in the simulated one. Hence, these results suggest that charge loss by the capsid is promoted by an external electric field.

It is possible that discrimination could influence the intensities in the frequency shift histogram. For example, if charge loss changed an ion's energy or trajectory so that it was not trapped for the full ~3 s, the ion would not be included in these results. If those events occurred preferentially in a particular part of the trap, the intensities in the frequency shift histogram would be skewed. However, the ion energies usually change by less than 1 eV/z during the trapping event, and remain within the energy bandwidth of the trap. The change in an ion's trajectory from loss of mass and charge should also be small, and unlikely to affect the ion's ability to be trapped because there are restoring fields in the trap to correct for small changes in trajectory. Finally, the frequency shift histogram in Figure 3a is depleted in regions of both high and low potential where the changes in the oscillation frequency are largest and smallest, and it is enhanced between these extremes. This is incompatible with discrimination playing a significant role.

Knowing that the mass loss associated with each charge loss is around 1000 Da, the total mass loss can be calculated for each ion. The total mass loss is the sum of the mass lost with each charge and the mass lost by gradual evaporation, which is modeled by Equation 5. Figure 4 shows histograms of total mass loss for ions that undergo a charge loss (solid black line) and for ions that did not (solid red line). In both cases, the most frequent mass loss (the peak in the distribution) is at around 20 kDa, but there are significant tails to larger mass losses that extend up to around 100 kDa. On average, ions that do not undergo a charge loss lose around 31 kDa when trapped, whereas ions that lose at least one charge lose around 36 kDa. The latter ions lose more mass in part because of the mass associated with the charge loss, but those ions also lose more to evaporation.

As noted above, it is anticipated that the ions studied here are generated by the charge residue model where droplets evaporate away and deposit their leftover charge on the ions. The HBV capsids were electrosprayed from a 100 mM ammonium acetate solution. In the final stages of solvent evaporation, the residue will become enriched in ammonium acetate and acetic acid as water and ammonia are the most volatile components. The ion no longer has a liquid water layer and charge loss can no longer follow the Rayleigh picture of electrostatic repulsion competing with surface tension. Loss of single charges, one at a time, is a characteristic of the IEM, though the ions are not being ejected from a liquid droplet in this case.

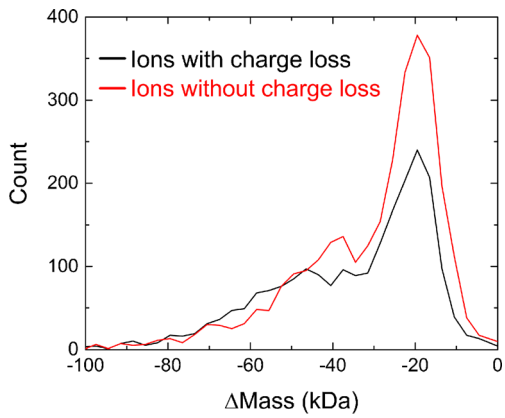

Figure 4. Histograms of total mass lost during 3 s trapping time. The solid black line shows results for ions that do lose a charge and the solid red line shows results for ions that do not lose a charge

However, it seems likely that field emission is ultimately responsible for the charge loss from the capsid ions.

Ammonia has a higher proton affinity than water [42]; thus NH_4^+ is most likely the charge carrier. The mass lost with the charge probably solvates the charge, lowering its energy. A mass of 1000 Da corresponds to around 13 ammonium acetate molecules or around 55 water molecules. For alkali halides, the $M^+(MX)_{13}$ cluster is particularly stable with a 3 × 3 × 3 cubic structure [43–45]. However, we cannot confirm that this is a prominent species for the ejected ions. The IEM involves loss of solvated ions [15, 16]. Increasing the amount of solvation lowers the energy of the charge but increases the surface energy. A balance between these two effects determines the optimum size of the solvated ion [16]. The results reported here are also consistent with molecular dynamics (MD) simulations of the final stage in the evolution of electrospray droplets [46–50]. In the MD simulations, the droplets undergo multiple losses of single solvated charges with solvent losses comparable to those found here.

The average charge on the $T = 4$ capsids that lose charge is 140 e, which leads to an electric field of around 8×10^8 V/m at the capsid surface. This is slightly smaller than the field usually associated with ion emission (10^9 V/m) [16] but as noted above, the ions are not being emitted from a liquid droplet. The field at the capsid surface is much larger than the maximum electric field in the trap (10^4 V/m), so how can such a small external field promote ion emission? Multiply charged ions are metastable. There is an energy barrier associated with loss of a charge, and the process is expected to be thermally activated [15]. The external field will slightly lower the activation barrier for some configurations, and a small difference in the activation barrier makes a large difference to the rate constant for field emission.

As noted in the Introduction, charge state resolution in the *m*/*z* spectrum is not obtained for megadalton-sized ions, a problem that is usually attributed to adduct formation. The results presented here suggest another contributor: charge loss promoted by external electric fields. The electric fields in the acceleration region of typical time-of-flight mass spectrometer are more than an order of magnitude larger than the 10^4 V/m experienced by the ions in this study. Thus the ions may lose charge as they accelerate, and after acceleration their charge and energy will be mismatched, leading to a loss of resolution in the *m*/*z* spectrum.

Conclusions

CDMS has been used to track the mass and charge of individual HBV capsids for 3 s. All ions gradually lose mass (presumably solvent, water, and/or salt). The total mass lost during the 3 s trapping period peaks at around 20 kDa, though some ions lose much more. Over 40% of the ions also lose a single charge combined with a mass of around 1000 Da (again, presumably solvent). These mass and charge loss processes represent the final stages in the evolution of megadalton ions after being electrosprayed. The loss of single charges is characteristic of the IEM. However, the capsids are almost certainly charged by the CRM and the charge should not be high enough to generate a large enough electric field to drive ion emission. The loss of a substantial amount of solvent along with the charge is consistent with recent MD simulations. The charge loss is promoted by external electric fields. This may contribute to the loss in *m*/*z* resolution that occurs for megadalton ions.

Acknowledgments

The authors are grateful for the support of the National Science Foundation through award CHE-1531823. They thank Dr. Lisa Selzer and Dr. Adam Zlotnick for providing the HBV sample.

References

1. Uetrecht, C., Versluis, C., Watts, N.R., Roos, W.H., Wuite, G.J.L., Wingfield, P.T., Steven, A.C., Heck, A.J.R.: High-resolution mass spectrometry of viral assemblies: molecular composition and stability of dimorphic hepatitis B virus capsids. Proc. Natl. Acad. Sci. **105**, 9216–9220 (2008)
2. Pierson, E.E., Keifer, D.Z., Contino, N.C., Jarrold, M.F.: Probing higher order multimers of pyruvate kinase with charge detection mass spectrometry. Int. J. Mass Spectrom. **337**, 50–56 (2013)
3. Hernandez, H., Robinson, C.V.: Determining the stoichiometry and interactions of macromolecular assemblies from mass spectrometry. Nat. Protoc. **2**, 715–726 (2007)
4. Lössl, P., Snijder, J., Heck, A.J.R.: Boundaries of mass resolution in native mass spectrometry. J. Am. Soc. Mass Spectrom. **25**, 906–917 (2014)
5. Keifer, D.Z., Pierson, E.E., Hogan, J.A., Bedwell, G.J., Prevelige, P.E., Jarrold, M.F.: Charge detection mass spectrometry of bacteriophage P22 procapsid distributions above 20 MDa. Rapid Commun. Mass Spectrom. **28**, 483–488 (2014)
6. Tahallah, N., Pinkse, M., Maier, C.S., Heck, A.J.R.: The effect of the source pressure on the abundance of ions of noncovalent protein assemblies in an electrospray ionization orthogonal time-of-flight instrument. Rapid Commun. Mass Spectrom. **15**, 596–601 (2001)
7. Chernushevich, I.V., Thomson, B.A.: Collisional cooling of large ions in electrospray mass spectrometry. Anal. Chem. **76**, 1754–1760 (2004)
8. van den Heuvel, R.H.H., van Duijn, E., Mazon, H., Synowsky, S.A., Lorenzen, K., Versluis, C., Brouns, S.J.J., Langridge, D., van der Oost, J., Hoyes, J., Heck, A.J.R.: Improving the performance of a quadrupole time-of-flight instrument for macromolecular mass spectrometry. Anal. Chem. **78**, 7473–7483 (2006)
9. Lorenzen, K., Versluis, C., van Duijn, E., van den Heuvel, R.H.H., Heck, A.J.R.: Optimizing macromolecular tandem mass spectrometry of large noncovalent complexes using heavy collision gases. Int. J. Mass Spectrom. **268**, 198–206 (2007)
10. Chowdhury, S.K., Katta, V., Chait, B.T.: An electrospray-ionization mass spectrometer with new features. Rapid Commun. Mass Spectrom. **4**, 81–87 (1990)
11. Wilm, M.S., Mann, M.: Electrospray and Taylor-cone theory, Dole's beam of macromolecules at last? Int. J. Mass Spectrom. **136**, 167–180 (1994)
12. Juraschek, R., Dülcks, T., Karas, M.: Nanoelectrospray—more than just a minimized-flow electrospray ionization source. J. Am. Soc. Mass Spectrom. **10**, 300–308 (1990)
13. Rayleigh, L.: XX. On the equilibrium of liquid conducting masses charged with electricity. Philos. Mag. Ser. 5 **14**, 184–186 (1882)
14. Fernandez de la Mora, J.: Electrospray ionization of large multiply charged species proceeds via Dole's charged residue mechanism. Anal. Chim. Acta **406**, 93–104 (2000)
15. Iribarne, J.V., Thomson, B.A.: On the evaporation of small ions from charged droplets. J. Chem. Phys. **64**, 2287–2294 (1976)

16. Thompson, B.A., Iribarne, J.V.: Field induced evaporation from liquid surfaces at atmospheric pressure. J. Chem. Phys. **71**, 4451–4463 (1979)
17. Fenn, J.B., Rosell, J., Meng, C.K.: In electrospray ionization, how much pull does an ion need to escape its droplet prison? J. Am. Soc. Mass Spectrom. **8**, 1147–1157 (1997)
18. Hogan, C.J., Carroll, J.A., Rohrs, H.W., Biswas, P., Gross, M.L.: Charge carrier field emission determines the number of charges on native state proteins in electrospray ionization. J. Am. Chem. Soc. **130**, 6926–6927 (2008)
19. Hogan, C.J., Carroll, J.A., Rohrs, H.W., Biswas, P., Gross, M.L.: Combined charged residue-field emission model of macromolecular electrospray ionization. Anal. Chem. **81**, 369–377 (2009)
20. Zlotnick, A., Cheng, N., Conway, J.F., Booy, F.P., Steven, A.C., Stahl, S.J., Wingfield, P.T.: Dimorphism of hepatitis B virus capsids is strongly influenced by the C-terminus of the capsid protein. Biochemistry **35**, 7412–7421 (1996)
21. Shockley, W.: Currents to conductors induced by a moving point charge. J. Appl. Phys. **9**, 635–636 (1938)
22. Weinheimer, A.J.: The charge induced on a conducting cylinder by a point charge and its application to the measurement of charge on precipitation. J. Atmos. Ocean. Technol. **5**, 298–304 (1988)
23. Shelton, H., Hendricks, J.C.D., Wuerker, R.F.: Electrostatic acceleration of microparticles to hypervelocities. J. Appl. Phys. **31**, 1243–1246 (1960)
24. Fuerstenau, S.D., Benner, W.H.: Molecular weight determination of megadalton DNA electrospray ions using charge detection time-of-flight mass spectrometry. Rapid Commun. Mass Spectrom. **9**, 1528–1538 (1995)
25. Schultz, J.C., Hack, C.A., Benner, W.H.: Mass determination of megadalton-DNA electrospray ions using charge detection mass spectrometry. J. Am. Soc. Mass Spectrom. **9**, 305–313 (1998)
26. Doussineau, T., Kerleroux, M., Dagany, X., Clavier, C., Barbaire, M., Maurelli, J., Antoine, R., Dugourd, P.: Charging megadalton poly(ethylene oxide)s by electrospray ionization. A charge detection mass spectrometry study. Rapid Commun. Mass Spectrom. **25**, 617–623 (2011)
27. Benner, W.H.: A gated electrostatic ion trap to repetitiously measure the charge and *m/z* of large electrospray ions. Anal. Chem. **69**, 4162–4168 (1997)
28. Contino, N.C., Jarrold, M.F.: Charge detection mass spectrometry for single ions with a limit of detection of 30 charges. Int. J. Mass Spectrom. **345/347**, 153–159 (2013)
29. Contino, N.C., Pierson, E.E., Keifer, D.Z., Jarrold, M.F.: Charge detection mass spectrometry with resolved charge states. J. Am. Soc. Mass Spectrom. **24**, 101–108 (2013)
30. Pierson, E.E., Contino, N.C., Keifer, D.Z., Jarrold, M.F.: Charge detection mass spectrometry for single ions with an uncertainty in the charge measurement of 0.65 e. J. Am. Soc. Mass Spectrom. **26**, 1213–1220 (2015)
31. Keifer, D.Z., Shinholt, D.L., Jarrold, M.F.: Charge detection mass spectrometry with almost perfect charge accuracy. Anal. Chem. **87**, 10330–10337 (2015)
32. Cheng, X., Bakhtiar, R., Van Orden, S., Smith, R.D.: Charge-state shifting of individual multiply-charged ions of bovine albumin dimer and molecular weight determination using an individual-ion approach. Anal. Chem. **66**, 2084–2087 (1994)
33. Smith, R.D., Cheng, X., Bruce, J.E., Hofstadler, S.A., Anderson, G.A.: Trapping, detection and reaction of very large single molecular ions by mass spectrometry. Nature **369**, 137–139 (1994)
34. Cheng, X., Camp, D.G., Wu, Q., Bakhtiar, R., Springer, D.L., Morris, B.J., Bruce, J.E., Anderson, G.A., Edmonds, C.G., Smith, R.D.: Molecular weight determination of plasmid DNA Using Electrospray Ionization Mass Spectrometry. Nucleic Acids Res. **24**, 2183–2189 (1996)
35. Bell, D.M., Howder, C.R., Johnson, R.C., Anderson, S.L.: Single CdSe/ZnS nanocrystals in an ion trap: charge and mass determination and photophysics evolution with changing mass, charge, and temperature. ACS Nano **8**, 2387–2398 (2014)
36. Howder, C.R., Bell, D.M., Anderson, S.L.: Optically detected, single nanoparticle mass spectrometer with pre-filtered electrospray nanoparticle source. Rev. Sci. Instrum. **85**, 014104 (2014)
37. Howder, C.R., Long, B.A., Bell, D.M., Anderson, S.L.: Thermally brightened CdSe/ZnS quantum dots as noncontact probes for surface chemistry studies of dark nanoparticles trapped in the gas phase. J. Phys. Chem. C **119**, 14561–14570 (2015)
38. Chen, R., Cheng, X., Mitchell, D.W., Hofstadler, S.A., Wu, Q., Rockwood, A.L., Sherman, M.G., Smith, R.D.: Trapping, detection, and mass determination of coliphage T4 DNA ions by electrospray ionization fourier transform ion cyclotron resonance mass spectrometry. Anal. Chem. **67**, 1159–1163 (1995)
39. Crowther, R.A., Kiselev, N.A., Böttcher, B., Berriman, J.A., Borisova, G.P., Ose, V., Pumpens, P.: Three-dimensional structure of hepatitis B virus core particles determined by electron cryomicroscopy. Cell **77**, 943–950 (1994)
40. Tolmachev, A.V., Chernushevich, I.V., Dodonov, A.F., Standing, K.G.: A collisional focusing ion guide for coupling an atmospheric pressure ion source to a mass spectrometer. Nucl. Instrum. Meth. Phys. Res. B **124**, 112–119 (1997)
41. Shin, H.T., Lee, Y.P., Jurng, J.: Spherical-shaped ice particle production by spraying water in a vacuum chamber. Appl. Therm. Eng. **20**, 439–454 (2000)
42. Lias, S.G., Liebman, J.F., Levin, R.D.: Evaluated gas phase basicities and proton affinities of molecules; heats of formation of protonated molecules. J. Phys. Chem. Ref. Data **13**, 695–808 (1984)
43. Campana, J.E., Barlak, T.M., Colton, R.J., DeCorpo, J.J., Wyatt, J.R., Dunlap, B.I.: Effect of cluster surface energies on secondary-ion-intensity distributions from ionic crystals. Phys. Rev. Lett. **47**, 1046–1049.
44. Pflaum, R., Pfau, P., Sattler, K., Recknagel, E.: Electron impact studies on sodium halide microclusters. Surf. Sci. **156**, 165–172 (1985)
45. Dugourd, P., Hudgins, R.R., Jarrold, M.F.: High resolution ion mobility studies of sodium chloride nanocrystals. Chem. Phys. Lett. **267**, 186–192 (1997)
46. Znamenskiy, V., Marginean, I., Vertes, A.: Solvated ion evaporation from charged water nanodroplets. J. Phys. Chem. A **107**, 7406–7412 (2003)
47. Marginean, I., Znamenskiy, V., Vertes, A.: Charge reduction in electrosprays: slender nanojets as intermediates. J. Phys. Chem. B **110**, 6397–6404 (2006)
48. Ahadi, E., Konermann, L.: Ejection of solvated ions from electrosprayed methanol/water nanodroplets studied by molecular dynamics simulations. J. Am. Chem. Soc. **133**, 9354–9363 (2011)
49. Konermann, L., McAllister, R.G., Metwally, H.: Molecular dynamics simulations of the electrospray process: formation of NaCl clusters via the charged residue mechanism. J. Phys. Chem. B **118**, 12025–12033 (2014)
50. McAllister, R.G., Metwally, H., Sun, Y., Konermann, L.: Release of native-like gaseous proteins from electrospray droplets via the charged residue mechanism: insights from molecular dynamics simulations. J. Am. Chem. Soc. **137**, 12667–12676 (2015)